BIOCHEMISTRY
including biophysical chemistry & molecular biology

Article

pubs.acs.org/biochemistry

Mechanism of Nucleated Conformational Conversion of Aβ42

Ziao Fu,[†] Darryl Aucoin,[†] Judianne Davis,[‡] William E. Van Nostrand,[‡] and Steven O. Smith*[,†]

[†]Department of Biochemistry and Cell Biology, Stony Brook University, Stony Brook, New York 11794-5215, United States
[‡]Departments of Neurosurgery and Medicine, Stony Brook University, Stony Brook, New York 11794-8122, United States

Supporting Information

ABSTRACT: Soluble oligomers and protofibrils of the Aβ42 peptide are neurotoxic intermediates in the conversion of monomeric Aβ42 into the amyloid fibrils associated with Alzheimer's disease. Nuclear magnetic resonance and Fourier transform infrared spectroscopy, along with single-touch atomic force microscopy, are used to establish the structural transitions involved in fibril formation. We show that under conditions favorable for the nucleated conformation conversion, the Aβ42 peptide aggregates into largely unstructured low-molecular weight (MW) oligomers that are able to stack to form high-MW oligomers and to laterally associate to form protofibrils. β-Sheet secondary structure develops during the irreversible lateral association of the oligomers. The first step in this conversion is the formation of an antiparallel β-hairpin stabilized by intramonomer hydrogen bonding. The antiparallel β-hairpins then associate into a cross β-sheet structure with parallel and in-register β-strands having intermonomer hydrogen bonding.

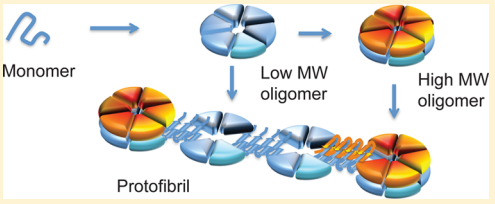

The amyloid-β (Aβ) peptides that form the amyloid fibrils associated with Alzheimer's disease (AD)[1] are generated by sequential proteolysis of the amyloid precursor protein (APP) by β- and γ-secretase.[2] The two predominant Aβ peptides, Aβ40 and Aβ42, differ by two amino acids, are soluble as monomers at low concentrations, and are normally cleared from the brain parenchyma.[3,4] With age or in the presence of familial mutations, the peptides aggregate, with the longer Aβ42 peptide having the highest frequency of occurrence in the insoluble plaques found in the brains of AD patients.[5] Despite intensive effort, the aggregation pathway from Aβ monomers to mature fibrils is not yet fully understood.

Two mechanisms are often proposed for fibril formation: nucleated polymerization and nucleated conformational conversion.[6−8] The classical mechanism involves polymerization of Aβ monomers to form a nucleus, which gives rise to fibrils through an elongation process involving monomer addition. The hallmark of this nucleated polymerization mechanism is the high level of monomers needed for elongation and the low level of off-pathway small soluble oligomers. This mechanism is favored at low concentrations of Aβ, which favor the monomeric species. The second general mechanism involves Aβ oligomers as intermediates in fibril formation. The oligomers form at higher Aβ concentrations and undergo a change in conformation to form protofibrils and then fibrils. The hallmark of the nucleated conformational conversion pathway is the high level of oligomers. The nature of the structural transition is a mystery, as is the role of monomeric Aβ in the elongation process. Nevertheless, as the Aβ oligomers have been implicated as the primary cause of neuronal cell death and synaptic dysfunction in AD,[9−12] the second pathway may strongly contribute to the progression of AD.

While the relative concentration of monomers and oligomers appears to strongly influence the mechanism for fibril formation, other factors are clearly at play, such as temperature. For example, at low Aβ concentrations (0.5−6 μM) and a high temperature (37 °C), Cohen et al.[6] have observed that soluble neurotoxic oligomers can be formed from monomeric Aβ through a fibril-catalyzed secondary nucleation reaction. Also, at high concentrations (160−200 μM) and a low temperature (15 °C), Clore and co-workers[13,14] observed a loss of NMR intensity in solutions of both monomeric Aβ40 and Aβ42 that they attributed to the formation of protofibrils in the absence of oligomeric intermediates.

The dual dependence of the monomer−oligomer equilibrium on temperature and concentration raises the possibility that the nucleated polymerization and conformational conversion mechanisms can occur in solution simultaneously.[15,16] The broad distributions of intermediates often observed during fibril formation[17] and the occurrence of off-pathway oligomers[18,19] may reflect the temperature and concentration regimes under which monomers and oligomers coexist.

In this study, we first take advantage of solution NMR spectroscopy to establish the interplay between concentration and temperature on oligomer formation to untangle nucleated conformational conversion from nucleated polymerization. We then rely on solution NMR to select a regime in which the nucleated conformational conversion mechanism is dominant to establish the structural changes occurring during fibril formation via oligomeric intermediates. The oligomers formed during the aggregation process are visualized using low-force, single-touch atomic force microscopy (AFM), and the structural changes that occur in the Aβ peptide are followed with circular dichroism (CD) and isotope-edited Fourier

Received: April 28, 2015
Revised: June 12, 2015
Published: June 12, 2015

DOI: 10.1021/acs.biochem.5b00467
Biochemistry 2015, 54, 4197−4207

transform infrared (FTIR) spectroscopy. The FTIR approach provides a sequence specific method for monitoring the changes in secondary structure as a function of aggregation state and reveals the structural transitions at the heart of the conformational conversion mechanism. Finally, we characterize the structure of the fibrils formed under both nucleated polymerization and conformational conversion using solid-state NMR spectroscopy.

MATERIALS AND METHODS

Preparation of Oligomers, Protofibrils, and Fibrils. Aβ42 peptides were synthesized using tBOC chemistry on an ABI 430A solid phase peptide synthesizer (Applied Biosystems, Foster City, CA) and purified by high-performance liquid chromatography (HPLC) using linear water/acetonitrile gradients containing 0.1% (v/v) trifluoroacetic acid. On the basis of analytical reverse phase HPLC, the purity of the peptides was at least 95%. The mass of the purified peptide was measured using matrix-assisted laser desorption or electrospray ionization mass spectrometry and was consistent with the calculated mass for the peptide. Peptides at a mass/charge ratio m/z 110 lower than that of the molecular ion [i.e., peptides that were synthesized with (randomly) one fewer amino acid] corresponded to <2% of the sample.

Purified, lyophilized Aβ42 (Keck Peptide Facility, Yale University, New Haven, CT) was dissolved in 100 mM NaOH at a concentration of 2.2 mM, then diluted in low-salt buffer (10 mM phosphate and 10 mM NaCl) at a low temperature (4 °C), and titrated to pH 7.4. The Aβ solutions were then filtered two times with 0.2 μm cellulose acetate filters to remove insoluble aggregates that can nucleate and influence aggregation. The final Aβ42 concentrations were then adjusted to the range of 10−200 μM. To initiate Aβ aggregation, the solutions of monomeric peptide at 4 °C were placed in a 37 °C incubator and slowly shaken. For AFM measurements and fluorescence measurements, aliquots of the peptide solution were removed at time points between 0 and 50 h. For solid-state NMR studies of the Aβ42 oligomer and protofibrils, aliquots of the peptide solution were removed at time points between 0 and 10 h and lyophilized. To prepare fibril samples, Aβ42 was allowed to incubate for 12 days, and then we used the fibril solution for seeded growth by sonicating, removing 5% of the sample, and adding monomeric Aβ. The sonication−seeding−growth sequence was repeated through 28 generations.

Atomic Force Microscopy. AFM images were obtained using a MultiMode microscope (Digital Instruments, Santa Barbara, CA) with a custom-built controller (LifeAFM, Port Jefferson, NY) that allows one low-force contact of the AFM tip to the sample surface per pixel. Supersharp silicon probes with a tip width of 3−5 nm (at a height of 2 nm) were modified for magnetic retraction by attachment of samarium cobalt particles. The oligomer diameters that are reported account for the width of the AFM probe tip.[20] Samples for AFM were diluted to a concentration of 0.5 μM deposited onto freshly cleaved ruby mica (S & J Trading, Glen Oaks, NY) and imaged under hydrated conditions.

Fluorescence Spectroscopy. Fluorescence experiments were performed using a Horiba Jobin Yvon Fluorolog FL3-22 spectrofluorimeter or a SpectraMax M2 microplate reader. For experiments on the FL3-22 spectrofluorimeter, at each time point, aliquots were taken and mixed with 30 μM 1-anilinonaphthalene-8-sulfonate (ANS) or thioflavin T to produce mixtures with a peptide:ANS ratio of 1:4.5, or a peptide:thioflavin T ratio of 1:20. ANS fluorescence emission spectra were recorded from 400 to 600 nm using an excitation wavelength of 349 nm. Thioflavin T fluorescence emission spectra were recorded from 475 to 550 nm using an excitation wavelength of 461 nm. For experiments on the SpectraMax M2 microplate reader, Aβ42 peptides were solubilized in 100 mM NaOH and diluted in low-salt phosphate buffer containing 50 μM thioflavin T to concentrations ranging from 10 to 200 μM and titrated to a pH of 7.4. Thioflavin T fluorescence was monitored every 15 s with excitation, emission, and automatic cutoff wavelengths of 446, 490, and 475 nm, respectively. Each experimental point is the mean of the fluorescence signal of at least five wells containing aliquots of the same solution.

Size Exclusion Chromatography (SEC). SEC was undertaken using an ÄKTA Purifier 10 (GE Healthcare, Piscataway, NJ) FPLC system with a Superdex 200 column having a 3−600 kDa molecular weight (MW) range. The ÄKTA purifier was kept at 4 °C to reduce the level of Aβ aggregation during the experiment. The samples were incubated at 37 °C while being shaken and then injected onto the Superdex column.

Fourier Transform Infrared (FTIR) Spectroscopy. The FTIR spectra were recorded from 400 to 4000 cm^{-1} on a Bruker IFS 66 V/S spectrometer equipped with a liquid N_2-cooled mercury cadmium telluride detector. The internal reflection element was a germanium ATR plate. Samples were prepared by spreading 50−100 μL of a peptide solution on the plate surface and by drying under N_2 or air.

Circular Dichroism (CD) Spectroscopy. CD spectra were recorded on an Olis RSM CD spectrophotometer (Olis Inc., Bogart, GA) using a 1 mm width quartz cuvette at an Aβ42 concentration of 200 μM.

Solution NMR Spectroscopy. NMR spectra of Aβ42 oligomers were recorded at 850 MHz on a Bruker AVANCE spectrometer with a TXI probe. NMR measurements were taken with standard 5 mm NMR tubes containing a Teflon tube liner (Norell, Inc.). $^{1}H-^{15}N$ HSQC spectra were recorded using pulse field gradient water suppression and GARP decoupling with the ^{1}H transmitter offset placed at the water frequency. For the two-dimensional (2D) data sets, 128 time increments were acquired in the indirect dimension with 16 scans per increment. Assignments were taken from the literature.[21,22]

Solid-State NMR Spectroscopy. Solid-state NMR experiments were performed at a ^{13}C frequency of 125 MHz on a Bruker AVANCE spectrometer. The MAS spinning rate was set to 9−11 kHz (±5 Hz). Ramped amplitude cross-polarization was used with a contact time of 2 ms. Two-pulse phase-modulated decoupling was used during the evolution and acquisition periods with a radiofrequency field strength of 80 kHz. Internuclear $^{13}C\cdots^{13}C$ distance constraints were obtained from 2D dipolar assisted rotational resonance (DARR) NMR experiments[23] using a mixing time of 600 ms.

RESULTS

Temperature Dependence of Nucleated Conformational Conversion. NMR spectroscopy provides a high-resolution approach for following the monomer concentration over a wide range of concentrations and temperatures. At 4 °C, Aβ42 is predominantly monomer at concentrations up to at least 200 μM.[24] The intensity of the NMR resonances in the $^{1}H-^{15}N$ HSQC spectrum of Aβ42 at 4 °C is a sensitive measure of monomeric peptide (Figure 1A). As the temper-

DOI: 10.1021/acs.biochem.5b00467
Biochemistry 2015, 54, 4197−4207

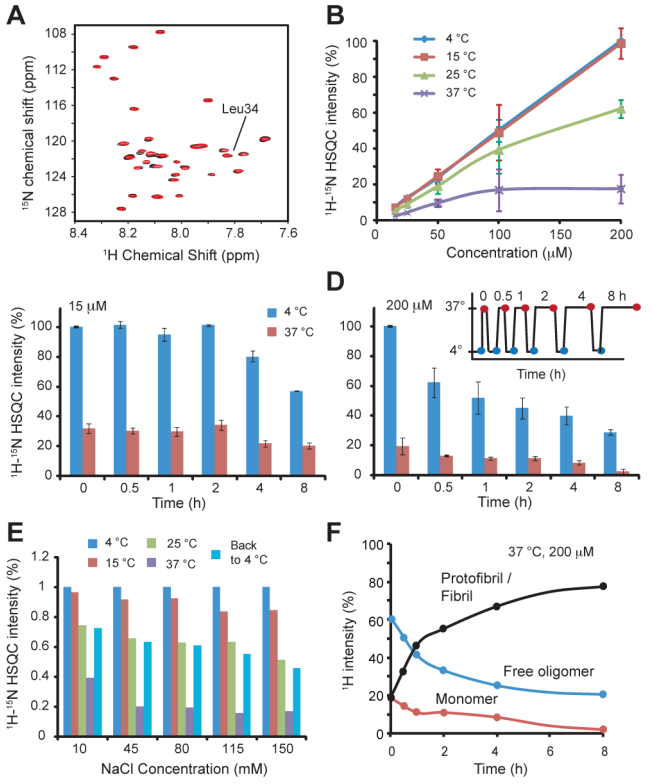

Figure 1. Monomer level that is a function of Aβ42 concentration and temperature. (A) ^{1}H−^{15}N HSQC NMR spectrum of monomeric (200 μM) Aβ42 obtained at 4 °C (black) overlaid with the HSQC NMR spectrum heated to 37 °C and recooled to 4 °C (red). The similar frequencies and intensities indicate that monomer structure is recovered after the heating−cooling cycle. (B) ^{1}H−^{15}N HSQC intensity of Aβ42 as a function of temperature and concentration obtained from a 200 μM stock solution of monomeric Aβ42 stabilized at 4 °C and diluted to 100, 50, 25, and 15 μM. The solutions were warmed to either 15, 25, or 37 °C, and HSQC spectra were recorded within 10 min of reaching the target temperature. The intensities are normalized to 200 μM Aβ42 at 4 °C. The results were averaged from three experiments. (C) ^{1}H−^{15}N HSQC intensity of Aβ42 as a function of incubation time. The intensity of 15 μM monomeric Aβ42 was first obtained at 4 °C, and then the temperature was changed to 37 °C and the intensity remeasured after delays of 0, 0.5, 1, 2, 4, and 8 h (red bars). After each 37 °C spectrum had been acquired, the temperature was cycled back to 4 °C and a spectrum collected (blue bars). The inset in panel D shows the warm−cool cycling scheme used for the 15 and 200 μM samples. (D) Same as panel C but starting with 200 μM monomeric Aβ42. (E) Dependence of HSQC intensity on salt concentration. In these experiments, monomeric Aβ42 (200 μM) was prepared at a given salt concentration at 4 °C. After the 4 °C HSQC spectrum had been recorded, the sample was heated to a new temperature and allowed to equilibrate for 5 min and the HSQC spectrum was collected. After the 37 °C spectrum was obtained, the sample was cooled to 4 °C for a final spectrum. In panels B−E, the intensity was measured of the Leu34 ^{1}H−^{15}N resonance, which was representative of the overall intensity of the HSQC spectra. The results represent the average and standard deviation from three experiments. (F) Time courses of monomer, free oligomer, and protofibril/fibril formation and decay on the basis of NMR intensities. The monomer concentration is taken from the ^{1}H−^{15}N HSQC intensity as a function of incubation time. The free oligomer concentration is taken from the methyl resonance intensity (minus the monomer concentration). The increase in the protofibril and fibril time course is inferred from the decrease in monomers and free oligomers. The experimental error is presented in panel D and Figure 1 of the Supporting Information.

ature is increased, Aβ42 aggregates and the intensity in the HSQC NMR spectrum decreases due to line broadening.[25] Figure 1B illustrates the extent of monomer loss as a function of concentration and temperature. At 4 and 15 °C, there is very little loss of intensity as the concentration increases. Substantial loss is observed at 25 and 37 °C. At the higher concentrations, only 15−20% of the total Aβ remains monomeric when the temperature is increased from 4 to 37 °C. The strong dependence of Aβ aggregation on temperature suggests that the hydrophobic effect is the driving force for monomer association.[26]

Clues about the nature of the aggregation process can be obtained by determining whether monomer association is reversible.[25] As stable β-sheet structure forms within the Aβ oligomers and protofibrils at 37 °C, it will not be possible to shift these structures back to monomers by lowering the temperature. We find that the aggregation induced at 37 °C is partly reversible at low concentrations (15 μM) of Aβ42 if the temperature is returned to 4 °C within the first few hours of incubation (Figure 1C). In these experiments, the intensity was first measured at 4 °C and then at 37 °C and remeasured after delays of 0, 0.5, 1, 2, 4, and 8 h (red bars) (see the inset of Figure 1D). Cooling the sample back to 4 °C after each heating cycle allows us to establish the percentage of Aβ42 that is able to revert to monomer (blue bars, Figure 1C,D) as a function of time.

In contrast, at a high concentration (200 μM) only a fraction of the Aβ42 reverts to monomer when the temperature is shifted back to 4 °C, and this fraction decreases as a function of the incubation time (Figure 1D). While the loss of monomer intensity is strongly influenced by the temperature and concentration, there is much less of a dependence on other factors, such as the salt concentration (Figure 1E). Importantly, the loss of the reversible transition indicates that the Aβ oligomers are changing structure as a function of time prior to their conversion into fibrils.

Concentration Dependence of Nucleated Conformational Conversion. The predominant Aβ oligomers formed at early times in the aggregation pathway at high concentrations are dimers, tetramers, pentamers, and hexamers.[27−29] We observe a rapid loss of intensity in the HSQC spectrum, despite the fact that these low-MW oligomers should be observable by NMR. To assess the fate of monomeric Aβ and the time course for the appearance of these oligomers, we undertook a series of additional experiments.

First, we measured the ^{1}H NMR intensity of the methyl group protons as a function of incubation time and Aβ concentration using one-dimensional NMR experiments. Because of rapid axial rotation of methyl groups, the CH_3 signal intensity is lost more slowly than the backbone ^{1}H−^{15}N intensity in the 2D HSQC NMR experiment. At 200 μM (37 °C), we retain ∼65% of the methyl ^{1}H NMR intensity after incubation for 1 h (Figure 1 of the Supporting Information). We attribute the observed methyl group intensity to monomeric Aβ42 (∼15% on the basis of Figure 1D) and low-MW oligomers (∼50%). Diffusion measurements by NMR are consistent with these oligomers being the size of pentamers and hexamers, and AFM measurements show that the low-MW oligomers are the most abundant free oligomers for the first 4−5 h after the start of incubation.[24] Approximately 35% of the methyl group ^{1}H intensity is not recoverable, which we attribute to low-MW oligomers that have associated to form higher-order complexes. (The mechanism of association is

DOI: 10.1021/acs.biochem.5b00467
Biochemistry 2015, 54, 4197−4207

discussed below.) At 15 μM (37 °C), there is a 2−3 h lag before a significant loss of methyl group ^{1}H intensity can be observed (data not shown).

In Figure 1F, we summarize the results of the quantitative NMR analysis. At 37 °C and 200 μM, the sample is ∼20% monomer and 80% oligomer. (The oligomer population is further divided into free oligomer and oligomers that are associated as protofibrils; see Discussion.) As a function of incubation time, the monomer and free oligomer concentrations decrease as protofibrils and fibrils form. (Here, the protofibril−fibril concentration is defined as the fraction that is not free monomer or free oligomer.)

Second, we followed the fluorescence of thioflavin T as a function of time. Thioflavin T exhibits a strong increase in fluorescence upon binding to amyloid fibrils. In Figure 2A, a lag

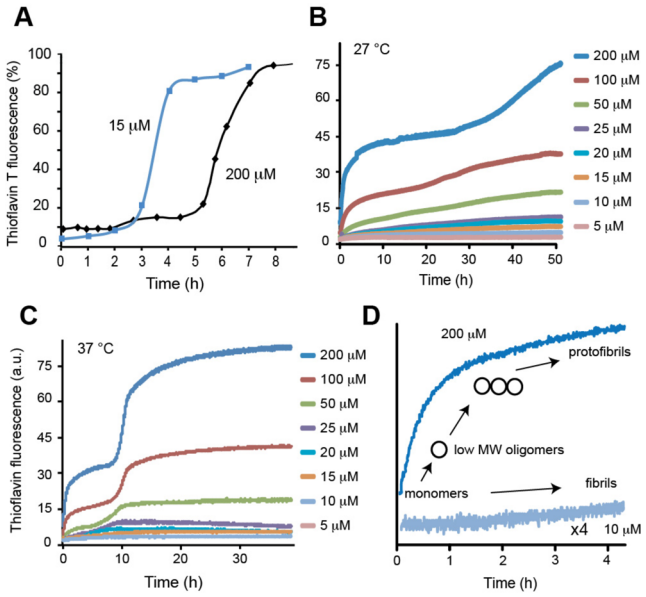

Figure 2. Thioflavin T fluorescence of Aβ42 as a function of concentration and incubation time. (A) Thioflavin T fluorescence of Aβ42 at 37 °C as a function of concentration. The curves obtained at 15 and 200 μM Aβ42 were obtained after diluting the samples to 1.5 μM prior to measurement. (B) Thioflavin T fluorescence of Aβ42 at 27 °C as a function of concentration obtained using a plate reader. The sample concentration was not diluted for fluorescence measurements. (C) Thioflavin T fluorescence of Aβ42 at 37 °C as a function of concentration obtained using a plate reader. The sample concentration was not diluted for fluorescence measurements. (D) Expansion of the thioflavin T fluorescence curves obtained in panel B at 10 and 200 μM Aβ42 and 37 °C. The fluorescence increases sharply at the higher concentration as the concentration rises above ∼20−30 μM. We attribute this increase in fluorescence to the lateral association of oligomers. Decreasing the concentration reduces this fluorescence, and a shift of Aβ back to monomers and low-MW oligomers that are not laterally associated is observed by NMR and SEC.

phase in thioflavin T fluorescence is observed before a sharp rise after ∼3−4 h at 15 μM and ∼6−7 h at 200 μM. The increase in thioflavin T fluorescence after ∼6−7 h at the higher concentration shows that the loss of methyl group ^{1}H intensity precedes fibril formation. It is important to note that in these experiments, the sample was diluted from 200 to 1.5 μM just prior to the fluorescence measurements.

Because the dilution of Aβ42 in the fluorescence measurements may alter the monomer−oligomer equilibrium (i.e., compare panels C and D of Figure 1), panels B and C of Figure 2 present the changes in thioflavin T fluorescence as a function of concentration at 27 and 37 °C, respectively, using a plate reader, which facilitates fluorescence measurements at high Aβ42 concentrations. At high concentrations, there is a rapid increase in thioflavin T fluorescence followed by a plateau before a second rise in fluorescence. The initial rise is not seen if the solution is first diluted (as in Figure 2A). The loss of fluorescence intensity upon dilution argues that the early intensity increase in panels B and C of Figure 2 at high concentrations is not due to fibril formation. A rapid change in fluorescence of Aβ42 labeled with tetramethylrhodamine has previously been observed.[30] However, these measurements with Aβ42 at low concentrations (0.5−4 μM) are associated with the rapid association of monomers to dimers and trimers.

We attribute the initial rise in thioflavin T fluorescence to the weak association of Aβ oligomers at early times in the aggregation process. The size of particles and the influence of dilution can also be assessed using size exclusion chromatography (SEC). SEC chromatograms of Aβ42 often exhibit two major peaks: one peak with a long elution time [∼17 mL (Figure 3A)] corresponds to monomers and free oligomers, and one peak with a short elution time [∼8 mL (Figure 3B)] is typically attributed to protofibrils. The change in peak intensities as a function of incubation time (Figure 3E) shows that the rise in the protofibril concentration and the decay in the monomer and free oligomer concentrations determined by SEC roughly correspond to those determined by NMR spectroscopy. Importantly, we are able to reverse the association of 200 μM Aβ42 for up to ∼6 h at 37 °C (Figure 3C,D) in a similar fashion as shown using NMR spectroscopy. During this time period, we predominantly observe protofibrils, but not fibrils, by TEM. At later times (>6 h), we attribute the increase in thioflavin T fluorescence to fibril formation.

As the concentration of Aβ42 is decreased (Figure 2B,C), the rapid, early increase in thioflavin T fluorescence is reduced. At low concentrations, we observe only a single rise in fluorescence after a lag phase (see Figure 2C, bottom trace). The changes in thioflavin kinetics with concentration and temperature suggest different aggregation mechanisms. One interpretation is that in the low-concentration region fibril formation occurs via nucleated polymerization, while in the high-concentration region oligomer-mediated nucleated conformational conversion is the predominant pathway (see Discussion).

Lateral Association of Low- and High-MW Oligomers Produces Protofibrils. To address the species being formed in the initial rise phase and in the lag phase before the final increase in thioflavin T fluorescence at 200 μM Aβ, we use single-touch atomic force microscopy (AFM). Single-touch AFM measures heights using a single, low-force contact per pixel and thus has advantages over conventional tapping mode AFM in terms of a higher resolution and a reduced level of sample distortion.[31]

The concentration needed to observe isolated oligomers and fibrils by AFM is on the order of ≤1 μM. As a result, we incubate Aβ over the concentration range of 10−200 μM, as in the NMR experiments, and then dilute the sample to 0.5−1 μM for observation. We have previously reported on the aggregation pathway of Aβ42 using AFM at an Aβ concentration of 16 μM.[31] In this concentration regime, where we propose nucleated polymerization dominates the aggregation process, we found that at early times (<6 h),

DOI: 10.1021/acs.biochem.5b00467
Biochemistry 2015, 54, 4197−4207

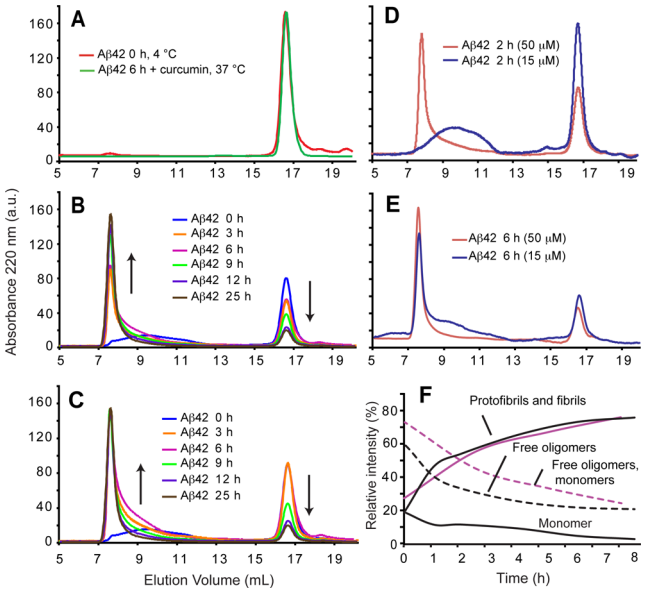

Figure 3. Size exclusion chromatography of Aβ42 as a function of concentration and incubation time. (A) The Aβ42 monomer prepared in low-salt buffer [10 mM NaCl and 10 mM phosphate (pH 7.4)] and stabilized at 4 °C elutes in the band at ~17 mL (red trace). NMR diffusion and relaxation measurements show that the 4 °C sample contains monomeric Aβ42 (see Figure 4 of the Supporting Information of ref 24). Similarly, incubation of Aβ42 with curcumin in a 1:1 molar ratio at 37 °C results in only a single band in the SEC chromatogram at 17 mL (green trace). We have shown that curcumin, which acts as a small molecule Aβ42 inhibitor, blocks the transition from low-MW oligomers to high-MW oligomers.[24] (B) Association of Aβ42 occurs rapidly after the sample of monomeric Aβ had been heated to 37 °C. Two bands are typically observed in the SEC chromatograms. The band at ~8 mL corresponds to high-MW Aβ aggregates and is typically associated with protofibrils, while the band at ~17 mL is associated with monomers and/or free oligomers. There is a rapid increase in the intensity of the band at 8 mL and a decrease in the intensity of the 17 mL band as a function of incubation time. In addition, we observe a shoulder on the 8 mL band that increases to a maximal value at ~6 h and then decays. (C) Same as in panel B with the chromatograms normalized to the protofibril peak at 8 mL to highlight the transient increase in the broad band at ~9 mL. (D and E) Influence of dilution upon aggregation. The 8 mL band can be largely reversed by dilution at early times (e.g., 2 h in panel D), whereas at later times, it cannot be reversed (e.g., 6 h in panel E). The intensities of the chromatograms for the 15 μM samples were scaled (50/15) for comparison with the 50 μM samples. (F) Comparison of the kinetics of Aβ42 aggregation using SEC (purple traces) and NMR (black traces). Both NMR and SEC show that there is immediate formation of aggregated Aβ upon heating the Aβ42 monomers (prepared at 4 °C) to 37 °C. The level of high-MW Aβ then increases with incubation time. In contrast, the level of monomers and free oligomers (dashed line) decreases with incubation time. We cannot distinguish monomers from free oligomers by SEC, as is possible using NMR spectroscopy.

monomers, dimers, and trimers gave rise to structures we termed unit protofibrils[31] with heights of ~2 nm and widths of 6–8 nm. The lengths of the unit protofibrils increase to >40 nm before their heights increase and the protofibrils resemble mature fibrils (Figure 4A). These structures differ from the laterally associated oligomers (described below) by their uniformly lower height and the absence of a punctate or "beads-on-a-string" structure. It is only when the sample concentration was increased that we observed the oligomeric species often described in the literature (see Figure 6 of ref 31).

We extend our AFM studies here by characterizing the structures that form at high Aβ42 concentrations (200 μM). At high concentrations and early incubation times, oligomers with diameters of 10–15 nm and heights of either ~1–2 or 3–5 nm are observed (Figure 4B). The difference in heights distinguishes two predominant oligomeric states, which we term low-MW oligomers and high-MW oligomers. We have observed that the number of low-MW oligomers decreases as a function of incubation time and that this decrease is correlated with an increase in the number of high-MW oligomers.[24] This correlation is consistent with the idea that the low-MW oligomers stack to form the high-MW oligomers.[24]

In contrast to the elongation of the unit protofibrils into fibrils at low concentrations, at high concentrations the protofibrils appear as laterally associated oligomers during the lag phase during incubation. These laterally associated oligomers appear in the same time frame as TEM images showing characteristic 100 nm protofibrils (Figure 2 of the Supporting Information). We present representative AFM images at 2 h (Figure 4C–E), 6 h (Figure 4F,G), and 8 h (Figure 4 H,I) to highlight several observations from a larger set of AFM images (see also Figure 3 of the Supporting Information). First, oligomer association occurs despite the dilution from 200 to 0.5 μM for AFM imaging. Second, even at short incubation times, we observe the lateral association of oligomers. In Figure 4C, a 500 nm square field is predominantly comprised of low-MW oligomers. In this field, there are several isolated (free) oligomers and several that have merged in a "beads-on-a-string" fashion. In Figure 4D, a 1000 nm square field reveals both low- and high-MW oligomers, and a single protofibril from this field is highlighted in Figure 4E, where high-MW oligomers clearly contribute to forming the protofibril. Fourth, there is an increase in the number of laterally associated oligomers as a function of incubation time. A quantitative analysis of the progression of free oligomers to laterally associated oligomers is presented in panels J and K of Figure 4. Comparison of the change in populations of free and laterally associated oligomers observed by AFM as a function of incubation time roughly corresponds to the populations determined by SEC. For example, at 6 h, the distribution between free and laterally associated oligomers is roughly 30% (free oligomer) and 70% (protofibril/fibril) by NMR and SEC, while it is 65% (free oligomer) and 35% (associated oligomers) by AFM. At the 6 h time point, roughly half of the oligomers are free and roughly half are associated. The relative increase in free oligomers versus associated oligomers observed by AFM is attributed to the extreme dilution needed for obtaining the AFM images. This correlation indicates that the associated oligomers are not a minor component of the total Aβ population and argues against mechanisms in which the free oligomers are off-pathway and simply serve to feed the monomer population that drives fibril growth.

We conclude that the protofibrils are formed from the association of both low- and high-MW oligomers, which then coalesce into fibrils. We propose that the growth of fibrils can occur by the addition of either monomers or oligomers. The NMR analysis (Figure 1D) shows that the monomer concentration is <10 μM after 8 h. However, this concentration is able to support growth by monomer addition, and we do observe a drop in the 20% monomer concentration at the beginning of incubation to zero after fibrils have formed.

DOI: 10.1021/acs.biochem.5b00467
Biochemistry 2015, 54, 4197–4207

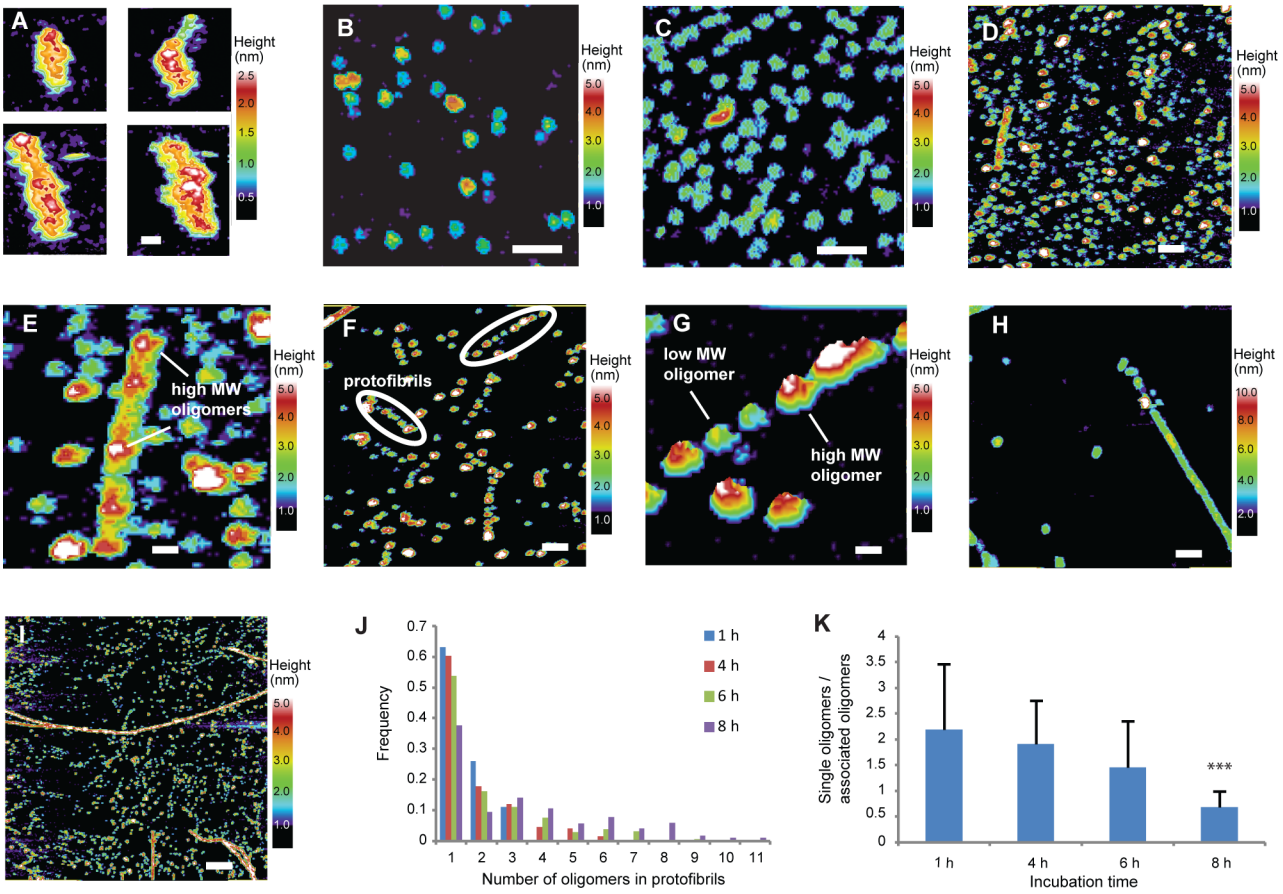

Figure 4. AFM images of Aβ42 as a function of concentration and incubation time. (A) Representative AFM images after incubation of Aβ42 at 37 °C for 4 h at 16 μM. The scale bar is 5 nm. (B) Representative AFM image of Aβ42 oligomers (200 μM). The AFM image was obtained starting with monomeric Aβ42 stabilized at 4 °C for 72 h in low-salt buffer (10 mM phosphate) prior to AFM measurements. The peptides are largely monomeric prior to warming the solution as it is layered on the mica grid for imaging. Warming to room temperature (i.e., the sample temperature is not controlled) causes a rapid conversion to Aβ42 oligomers with heights of ~1.5−2.5 nm. The scale bar is 100 nm. (C and D) Aβ42 oligomers after incubation for 2 h. Low-MW oligomers dominate in panel C. Associated oligomers (protofibrils) are observed in both panels. The scale bars are 100 nm. (E) Magnification of the protofibril in panel C. Height measurements along the protofibril suggest that it was formed from the association of low- and high-MW oligomers. (F) Aβ42 oligomers and protofibrils after incubation for 6 h. The Aβ42 oligomers form linear structures (circled) but remain as discrete disc-shaped objects (see Figure 3 of the Supporting Information). The linear structures have different orientations relative to the direction of scanning by the AFM probe, indicating that they are not artifacts of the scanning process. The scale bar is 100 nm. (G) Expanded view of an Aβ42 protofibril. This image is plotted in three-dimensional mode to highlight the differences in heights of the component oligomers. The scale bar is 20 nm. (H) AFM image of a mixture of Aβ42 oligomers and fibrils obtained after incubation for 8 h at 200 μM Aβ42. The scale bar is 100 nm. (I) AFM image of a mixture of Aβ42 oligomers, protofibrils, and fibrils obtained after incubation for 8 h under the same conditions described for panel H, but with a larger field of view. The scale bar is 300 nm. (J) Kinetics of Aβ42 association using AFM. The frequencies of single free oligomers are plotted relative to association of two or more oligomers as a function of incubation time. If there was a gap between two oligomers (as in panel G), the oligomers were counted as free. Oligomers that had merged and were not distinctly laterally associated were not counted. The number of oligomers counted for each time point was as follows: 1 h, 192; 4 h, 1622; 6 h, 1543; 8 h, 1068. (K) Ratio of the number of free oligomers vs associated oligomers as a function of incubation time. A single-tail unpaired t test reveals a significant difference ($p < 0.001$) only after 8 h.

Nevertheless, we conclude that the major mechanism for fibril growth under conditions of high concentrations and high temperatures is due to oligomer association. This conclusion is based on the observation of oligomers that associate in a "beads-on-a-string" fashion at high concentrations and temperatures, without the appearance of short fibrils that become longer as a function of incubation time. The latter dominate the AFM images under low-concentration conditions. Figure 4H shows a representative image suggesting the oligomers are able to associate to the growing ends of the fibrils. The ends of the fibrils consisting of recently associated oligomers likely require time to rearrange into the β-sheet structure present in the interior region of the fibril (see below).

Transient Antiparallel β-Strand Structure Precedes Fibril Formation. The results presented above provide the time courses for fibril formation at different temperatures and concentrations and allow us to select a regime in which nucleated conformational conversion is the dominant mechanism for fibril formation (Figure 5A). In this section, we use CD and FTIR spectroscopy to follow the changes in secondary structure at 37 °C and 200 μM Aβ42 as the monomeric peptide forms low-MW oligomers that laterally associate and/or stack to form high-MW oligomers.

CD spectra were first obtained as a function of Aβ42 aggregation (Figure 5B). The CD spectrum of the Aβ monomer (t = 0 h) exhibits a pronounced minimum at ~195−197 nm consistent with largely unstructured peptide.

DOI: 10.1021/acs.biochem.5b00467
Biochemistry 2015, 54, 4197−4207

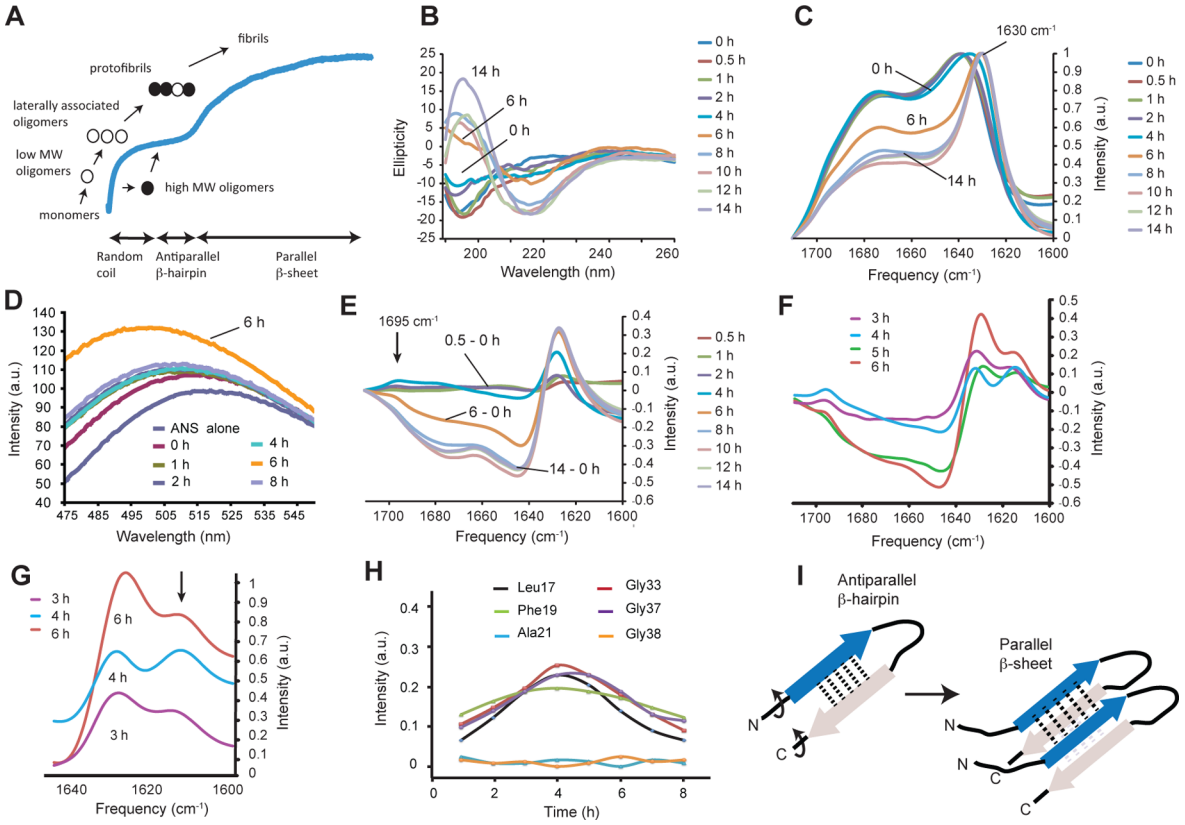

Figure 5. Changes in the secondary structure of Aβ42 as a function of incubation time. (A) Thioflavin T fluorescence curve showing the position of Aβ42 oligomers observed by AFM. (B) CD spectra and (C) FTIR spectra of Aβ42 obtained as a function of time at 37 °C and 200 μM Aβ42. (D) ANS fluorescence spectra from 0 to 8 h. No change in fluorescence was observed after ~10 h. The Aβ42 concentration was 200 μM. (E–G) FTIR difference spectra obtained by subtracting the spectrum at time zero from spectra obtained at each incubation time point. The FTIR spectra in panels F and G are of Aβ42 containing [1-^{13}C]Gly33. Panel G is an expansion of three of the spectra in panel F showing the relative intensity of the 1610 cm^{-1} band. The curves are shifted along the *y*-axis for the sake of clarity. (H) Plot of the intensity of the 1610 cm^{-1} band relative to that of the 1630 cm^{-1} band from Aβ42 containing either 1-^{13}C-labeled Leu17, Phe19, Ala21, Gly33, Gly37, or Gly38. (I) Conversion of antiparallel β-hairpin secondary structure to β-sheet secondary structure. Intramolecular hydrogen bonding stabilizes the antiparallel β-strands in the β-hairpin. Rotation of these β-strands allows the formation of intermolecular hydrogen bonds, which nucleates β-sheet secondary structure.

Nevertheless, the monomer is not fully random coil on the basis of solvent accessibility and the ability to bind small molecule inhibitors.[24] A partial structure of the Aβ40 monomer is consistent with residual structure in the monomer.[32] β-Sheet does not form significantly until after ~6 h. In the CD spectra, there is a shift of the negative ellipticity from ~200 to ~215 nm and an increase in the positive ellipticity at ~195 nm. The largest changes occur between the 6 and 8 h incubation time points. These changes are characteristic of a transition to β-sheet structure.

FTIR spectroscopy provides a complementary method for following the structural changes occurring during the aggregation process. As monomeric Aβ converts to fibrils, the FTIR spectra of Aβ42 exhibit a loss of the broad component between 1620 and 1700 cm^{-1} and a shift of the amide I peak from 1640 to 1630 cm^{-1} at ~6 h (Figure 5C). The broad component is associated with random coil structure, and the 1630 cm^{-1} band is a marker for β-sheet structure. The time course for these changes matches that observed by CD, namely that β-sheet structure does not appear until ~6 h, just before the rise in thioflavin T fluorescence between 6 and 8 h (Figure 2A). (Recall that the fluorescence increase at 6–8 h cannot be reversed by dilution and consequently corresponds to the formation of stable fibrils.) These observations allow us to draw several conclusions. First, the low-MW oligomers do not contain significant β-sheet structure. Second, the lateral association of low-MW oligomers within the first hour of incubation and the accompanying rise of thioflavin T fluorescence are not caused by fibril formation. There is no detectable β-sheet structure in the CD spectra of 200 μM Aβ42 in the first 30 min to 1 h when a very large increase in fluorescence is observed with the plate reader (Figure 2B,C).

The CD and FTIR data indicate that the conformational conversion from oligomers to fibrils occurs in the window where the laterally associated oligomers (i.e., protofibrils) begin to merge and cannot be reverted back to individual low-MW oligomers. This conversion is correlated with two additional observations. First, there is a rise in the fluorescence of ANS at ~6 h (Figure 5D). In contrast to thioflavin T fluorescence, kinetic studies have suggested that ANS can bind to Aβ42 oligomers.[33] When ANS is added to Aβ42 at 4 °C, no change is observed in the ANS fluorescence spectrum as a function of time (Figure 5 of the Supporting Information). This observation indicates that ANS does not bind to monomeric Aβ42. In contrast, at 37 °C a time-dependent shift in the ANS fluorescence spectrum is observed with a maximum at 6 h. Previous studies did not distinguish the binding of ANS to low- versus high-MW oligomers but did report a rise and fall of ANS fluorescence that correlated with toxicity.[33] We find that incubating Aβ42 with curcumin blocks the observed shift in

DOI: 10.1021/acs.biochem.5b00467
Biochemistry 2015, 54, 4197–4207

ANS fluorescence (Figure 4 of the Supporting Information), in agreement with the ability of curcumin to bind to Aβ42 monomers and low-MW oligomers and block the transition to the high-MW species.[24] The increase in ANS fluorescence at ~6 h supports the results from SEC (Figure 3) that there is a transient structural change that occurs just before the increase in thioflavin T fluorescence (and fibril formation).

Second, there is a transient increase in the intensity of a band at 1695 cm^{-1} in the FTIR spectra of Aβ42 (arrow, Figure 5E). This weak band is often obscured by the random coil band or side chain vibrations but can be enhanced in difference spectra (Figure 5E,F). The 1695 cm^{-1} frequency is often associated with antiparallel β structure.[34,35] In the FTIR spectra of Aβ42 obtained as a function of time, the intensity of the 1695 cm^{-1} band is strongest between ~4 and 6 h.

The weak intensity of the 1695 cm^{-1} band presents a problem in drawing strong conclusions about the type of β-sheet structure (parallel or antiparallel) that exists in Aβ protofibrils and fibrils. This is one of several problems in distinguishing antiparallel and parallel β-sheets in proteins using IR spectroscopy.[36] An alternative approach is to use isotope-edited FTIR spectroscopy where ^{13}C is incorporated into specific backbone carbonyl carbons along the Aβ sequence. The $^{13}C{=}O$ group shifts the amide vibration to lower frequencies, and both the frequency and intensity of the shifted vibrational band are sensitive to whether the $^{13}C{=}O$-labeled sites fall within parallel or antiparallel β-sheet structure.[37,38] FTIR spectra of Aβ42 containing 1-^{13}C-labeled Gly33 (Figure 5F,G) exhibit the transient appearance of an IR band at 1610 cm^{-1} that is not observed in the FTIR spectra of unlabeled Aβ42 (Figure 5C,E). The change in the intensity of this band reveals that antiparallel structure transiently appears between ~4 and 5 h, before the large increase in thioflavin T fluorescence associated with fibril formation. A similar increase is observed in Aβ42 individually containing 1-^{13}C-labeled Leu17, Phe19, or Gly37, but not at Ala21 or Gly38 (Figure 5H). The correlated rise and fall of the 1610 and 1695 cm^{-1} bands before the rise of thioflavin fluorescence at 6–7 h is attributed to antiparallel β-hairpin structure (Figure 5I). Neither of these bands is observed in fibrils shown to be parallel β-sheets by solid-state NMR (next section). Furthermore, the data argue that the transient appearance of the IR band at 1610 cm^{-1} is not associated with antiparallel β-sheet structure as this band appears in a time regime where the thioflavin T fluorescence does not change.

Concentration Dependence of Fibril Formation. One of the conclusions from the FTIR data is that the parallel, in-register fibrils characteristic of Aβ42 do not form prior to the rapid increase in thioflavin T fluorescence that occurs at ~7 h at 37 °C and 200 μM. In this section, we follow the formation of Aβ42 fibrils using solid-state NMR of specifically ^{13}C-labeled Aβ42. Figure 6A presents one-dimensional magic angle spinning (MAS) NMR spectra of Aβ42 oligomers and fibrils that are labeled at [5-^{13}C]Met35 and [2-^{13}C]Gly38. In the oligomers, the NMR resonances are broad, suggesting largely unstructured conformations. In the fibrils (grown at 200 μM Aβ42), the Met35 and Gly38 resonances narrow but split into multiple components indicating that different fibril forms are present. Seeding of the fibrils can produce a homogeneous population (Figure 6B). In this case, seeding retains the fibril form with the 15.1 ppm ^{13}C chemical shift for the [5-^{13}C]Met35 resonance. In contrast, fibrils formed at a low concentration (15 μM) are more homogeneous without seeding (Figure 6C); the fibrils exhibit predominantly the 17.4 ppm chemical shift for [5-^{13}C]Met35. The observation of a single population is consistent with more rapid fibril growth at low concentrations.

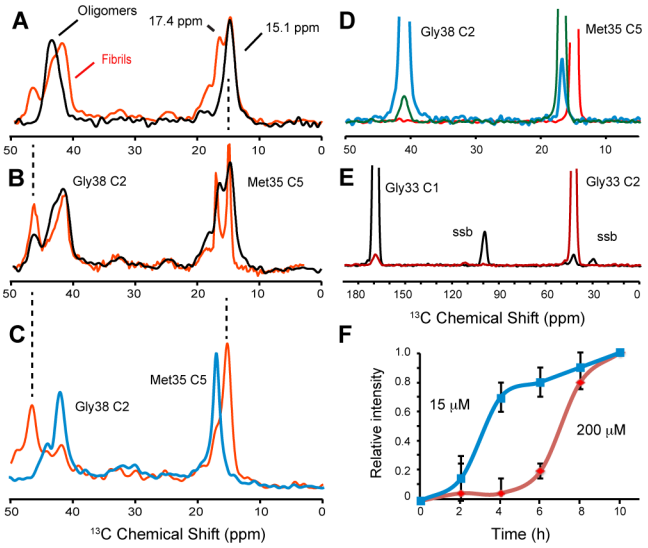

Figure 6. Parallel, in-register fibrils of Aβ42 form at both low and high Aβ concentrations. (A) One-dimensional solid-state magic angle spinning NMR spectra of Aβ42 oligomers (black) and fibrils (red) labeled at [5-^{13}C]Met35 and [2-^{13}C]Gly38. The oligomer and fibril spectra were obtained after incubation for 4 h and 4 days, respectively, at 37 °C with an Aβ concentration of 200 μM. (B) Four generations of repeated sonication–seeding–fibril growth narrow the NMR resonances (red) revealing two predominant fibril forms. (C) A homogeneous population of Aβ42 fibrils is obtained after 24 generations of repeated sonication–seeding–fibril growth cycles at 37 °C and 200 μM Aβ (red). In contrast, fibrils grown at 37 °C and 15 μM Aβ have a relatively well-defined structure without seeding (blue). (D) Rows extracted from two-dimensional DARR NMR spectra obtained using Aβ42 labeled with [5-^{13}C]Met35 and [2-^{13}C]Gly38. The fibril form characterized by the 17.4 ppm [5-^{13}C]Met35 resonance exhibits a strong cross-peak to [2-^{13}C]Gly38. (E) Rows extracted from two-dimensional DARR NMR spectra of Aβ42 fibrils obtained using an equimolar mixture of Aβ42 peptides labeled with either [1-^{13}C]Gly33 or [2-^{13}C]Gly33. The interfibril cross-peak observed is characteristic of parallel, in-register structure. Mature fibrils grown at both 15 and 200 μM exhibit Gly33–Gly33 cross-peaks. Spinning side bands (ssb) are labeled. (F) Time course of fibril formation in the 200 μM sample determined on the basis of an increase in intensity of the [2-^{13}C]Gly38 chemical shift at 46.5 ppm (red trace). The time course for fibril formation in the 15 μM sample was determined on the basis of the increase in the 17.4 ppm [5-^{13}C]Met35 resonance (blue trace). 2D NMR experiments with the fibrils at 10 h revealed the presence of an intense Met35–Gly38 cross-peak in fibrils exhibiting the 17.4 ppm [5-^{13}C]Met35 resonance.

The structures of the two different fibril forms observed above can be characterized using two-dimensional solid-state NMR spectroscopy. One marked difference between the fibril forms is the presence of a close contact between the Met35 methyl group and the Gly38 Cα atom in the fibril form with the 17.4 ppm Met35 chemical shift. This contact (reflected by the strong cross-peak observed in Figure 6D) is consistent with a sharp bend in the C-terminus of Aβ42.[39] A second difference is in the chemical shift of the Gly38 Cα atom, which differs by ~5 ppm (~41.8 and 46.5 ppm). In Figure 6F, we follow the formation of these two markers as a function of fibril formation. An increase in the intensity of the 46.5 ppm Gly38 resonance in

DOI: 10.1021/acs.biochem.5b00467
Biochemistry 2015, 54, 4197–4207

the 200 μM sample and that of the 17.4 ppm Met35 resonance in the 15 μM sample is consistent with the increase in thioflavin T fluorescence at the two concentrations (Figure 2C). At both concentrations, the mature fibrils have a parallel, in-register β-sheet structure as characterized using ^{13}C labels at Gly33 (Figure 6E).[40] In these experiments, we mix two populations of Aβ42 peptides; one population is labeled with [1-^{13}C]Gly33 and a second population with [2-^{13}C]Gly33.[40] In a parallel, in-register geometry, these two ^{13}C labels are within ~5.5 Å and generate a cross-peak in the two-dimensional NMR spectra as observed.

DISCUSSION

The studies undertaken here show that Aβ oligomers, the hallmark of the nucleated conformational conversion, rapidly form at temperatures above ~15 °C and have the ability to laterally associate into protofibrils in the process of forming fibrils. These studies address the mechanism of nucleated conformational conversion that dominates the pathway for Aβ aggregation at high temperatures and concentrations. We show that the lateral association is correlated with the conversion of random coil structure into β-sheet and propose that an intermediate step in this conversion is the transient formation of an antiparallel β-hairpin.

The first step in the pathway involving nucleated conformational conversion is association of monomeric Aβ to form low-MW oligomers. These oligomers can be converted back into monomeric Aβ at early time points in the pathway by lowering the temperature or concentration of the solution. If allowed to incubate, the low-MW oligomers both stack to form high-MW oligomers[24] and laterally associate.

The lateral association of Aβ42 oligomers is reflected in the "beads-on-a-string" morphology that is often observed in nascent protofibrils.[16,29,41] The AFM images provide direct evidence that both low-MW and high-MW oligomers can laterally associate and argue that these strings of oligomers are early forms of protofibrils at high Aβ concentrations. The results from ANS fluorescence, SEC, and FTIR spectroscopy all suggest a transition occurs just before rapid fibril growth. (A transient drop in the fluorescence of a novel FlAsH probe just prior to the rapid rise in thioflavin T fluorescence may reflect a similar intermediate structure upon oligomer association of Aβ40.[7]) We propose that this transition involves the formation of an antiparallel β-hairpin structure that exists before the conversion to β-sheet structure characteristic of mature fibrils.

The proposed β-hairpin structure associated with this transient intermediate state (Figure 5I) has intramolecular hydrogen bonding between a β-strand centered on the hydrophobic LVFF sequence and a β-strand in the hydrophobic GLMVG sequence at the C-terminus.[20] The isotope-edited FTIR studies indicate that Ala21 and Gly38 are not part of this antiparallel structure. The conversion to β-sheet structure involves rotation of the β-strands to allow intermolecular hydrogen bonds to form with a neighboring Aβ peptide.[42] It is known that in mature fibrils of Aβ42 the β-strands have a parallel orientation and the side chains are in-register.[40,43] As a result, the β-sheet is stabilized through intermolecular hydrogen bonds, as well as via both intramolecular and intermolecular packing interactions between the side chains in the β-strands. Consistent with this model, Tycko and Meredith[44] synthesized Aβ40-lactam(D23/K28), which contains a lactam bridge between the side chains of Asp23 and Lys28. Aβ40-lactam-(D23/K28) forms fibrils similar to those formed by Aβ40. However, fibril formation occurs without a lag phase and at a rate ~1000-fold greater than that of wild-type Aβ40. Similarly, we have found that in Aβ40 peptides with the Dutch (E22Q) and Iowa (D23N) mutations, which also exhibit rapid fibril formation, the antiparallel β-signature peaks appear after incubation for 1 h at 37 °C in a time window well before the increase in thioflavin T fluorescence associated with fibril formation (data not shown). This observation agrees with the studies of the Aβ40-lactam that formation of the antiparallel β-hairpin is a rate-determining step in fibril formation.

There is a wide range of data supporting the transient formation of a β-hairpin structure. One line of evidence comes from protein engineering studies in which β-hairpins are stabilized by an intramolecular disulfide bond.[45,46] The CC cross-link prevents intermolecular hydrogen bonding in the cross-β-sheet structures characteristic of mature fibrils. Aβ40-CC and Aβ42-CC both spontaneously form stable oligomers and protofibrils, but both are unable to convert into amyloid fibrils. Conformation specific antibodies used to detect Aβ aggregates *in vivo* indicate that the wild-type oligomer structure is preserved and stabilized in the Aβ-CC oligomers, which can also bind ANS. These experiments indicate considerable structural similarity with the laterally associated oligomers or protofibrils formed by wild-type Aβ42.

One of the motivations for understanding the mechanism of nucleated conformational conversion is that the soluble oligomers of Aβ are implicated in neuronal toxicity.[9−12] In this regard, it is important to note that the Aβ42-CC oligomers and protofibrils were found to be 50 times more potent inducers of neuronal apoptosis than Aβ42 monomers or fibrils.[45] We have previously shown that the time course of neuronal toxicity exhibits a maximal toxicity between 6 and 10 h,[24] which roughly correlates with the appearance of antiparallel β-hairpin structure and the transition from protofibrils to mature fibrils. In a similar fashion, Carulla and co-workers[12] observed an intermediate oligomeric species that is protected from hydrogen−deuterium exchange and correlates with neuronal cell death. The similarity between these observations and our studies suggests a similar toxic intermediate state in the conversion of largely unstructured Aβ oligomers to well-structured fibrils. These studies raise the question of the mechanism of oligomer and fibril formation *in vivo*. One possibility is that the equilibrium between soluble and membrane-bound Aβ favors the membrane-bound state, and Aβ that is not otherwise cleared or degraded forms membrane-bound oligomers that are in equilibrium with soluble oligomers. These oligomers can then form nuclei competent to form fibrils via monomer addition (nucleated polymerization) or can associate with other oligomers to form short protofibrils that convert into fibrils via nucleated conformational conversion.

The picture that emerges is one in which the hydrophobic effect drives the initial, rapid association of the hydrophobic sequences in the Aβ peptides. However, at high concentrations, this association is nonspecific and does not yield defined β-hairpin or β-sheet structure in the initial aggregates. The conversion to fibrils involves the untangling of the hydrophobic regions to first form an antiparallel β-hairpin structure prior to strand rotation in the conversion to cross β-sheet structure. The formation of the antiparallel β-hairpin (as opposed to antiparallel or parallel β-sheet) would be favored initially because the hydrogen bonding contacts are intramolecular as opposed to intermolecular. At high Aβ concentrations, a transient state characterized by an increase in ANS fluorescence

DOI: 10.1021/acs.biochem.5b00467
Biochemistry 2015, 54, 4197−4207

and antiparallel structure is associated with neuronal toxicity.[12,33] The antiparallel β-hairpins may occur in free oligomers or in laterally associated oligomers that have not merged into well-defined cross β-sheet consistent with both soluble oligomers[9−12] and protofibrils[47] conveying neuronal toxicity. At least two different fibril forms are observed at high concentrations, while a single form dominates at low concentrations. The differences in fibril structure obtained at low (15 μM) and high (200 μM) concentrations are consistent with the overall conclusion that nucleated conformational conversion dominates at high concentrations (>20−30 μM) and nucleated polymerization dominates at low concentrations.

■ ASSOCIATED CONTENT

Supporting Information

Methyl ^{1}H NMR intensity as a function of time (Figure 1), transmission electron microscopy of Aβ42 oligomers, protofibrils, and fibrils (Figure 2), AFM of Aβ42 oligomers, protofibrils, and fibrils (Figure 3), and ANS fluorescence of Aβ42 (Figure 4). The Supporting Information is available free of charge on the ACS Publications website at DOI: 10.1021/acs.biochem.5b00467.

■ AUTHOR INFORMATION

Corresponding Author

*E-mail: steven.o.smith@stonybrook.edu. Telephone: (631) 632-1210. Fax: (631) 632-8575.

Funding

This work was supported by grants from the National Institutes of Health (RO1-AG027317 to S.O.S. and R21-NS85361 to W.E.V.N.) and the Cure Alzheimer's Fund to W.E.V.N.

Notes

The authors declare no competing financial interest.

■ ABBREVIATIONS

Aβ, amyloid-β; AD, Alzheimer's disease; AFM, atomic force microscopy; ANS, 1-anilinonaphthalene-8-sulfonate; APP, amyloid precursor protein; CD, circular dichroism; DARR, dipolar assisted rotational resonance; FTIR, Fourier transform infrared; HPLC, high-performance liquid chromatography; HSQC, heteronuclear single-quantum correlation; MW, molecular weight; NMR, nuclear magnetic resonance; SEC, size exclusion chromatography; TEM, transmission electron microscopy.

■ REFERENCES

(1) Selkoe, D. J. (2001) Alzheimer's disease: Genes, proteins, and therapy. *Physiol. Rev. 81*, 741−766.

(2) De Strooper, B., Vassar, R., and Golde, T. (2010) The secretases: Enzymes with therapeutic potential in Alzheimer disease. *Nat. Rev. Neurol. 6*, 99−107.

(3) Selkoe, D. J. (2001) Clearing the brain's amyloid cobwebs. *Neuron 32*, 177−180.

(4) Zlokovic, B. V., Yamada, S., Holtzman, D., Ghiso, J., and Frangione, B. (2000) Clearance of amyloid β-peptide from brain: Transport or metabolism? *Nat. Med. 6*, 718.

(5) Portelius, E., Bogdanovic, N., Gustavsson, M., Volkmann, I., Brinkmalm, G., Zetterberg, H., Winblad, B., and Blennow, K. (2010) Mass spectrometric characterization of brain amyloid β isoform signatures in familial and sporadic Alzheimer's disease. *Acta Neuropathol. 120*, 185−193.

(6) Cohen, S. I. A., Linse, S., Luheshi, L. M., Hellstrand, E., White, D. A., Rajah, L., Otzen, D. E., Vendruscolo, M., Dobson, C. M., and Knowles, T. P. J. (2013) Proliferation of amyloid-β 42 aggregates occurs through a secondary nucleation mechanism. *Proc. Natl. Acad. Sci. U.S.A. 110*, 9758−9763.

(7) Lee, J., Culyba, E. K., Powers, E. T., and Kelly, J. W. (2011) Amyloid-β forms fibrils by nucleated conformational conversion of oligomers. *Nat. Chem. Biol. 7*, 602−609.

(8) Cheon, M., Chang, I., Mohanty, S., Luheshi, L. M., Dobson, C. M., Vendruscolo, M., and Favrin, G. (2007) Structural reorganisation and potential toxicity of oligomeric species formed during the assembly of amyloid fibrils. *PLoS Comput. Biol. 3*, 1727−1738.

(9) Lambert, M. P., Barlow, A. K., Chromy, B. A., Edwards, C., Freed, R., Liosatos, M., Morgan, T. E., Rozovsky, I., Trommer, B., Viola, K. L., Wals, P., Zhang, C., Finch, C. E., Krafft, G. A., and Klein, W. L. (1998) Diffusible, nonfibrillar ligands derived from Aβ1−42 are potent central nervous system neurotoxins. *Proc. Natl. Acad. Sci. U.S.A. 95*, 6448−6453.

(10) Walsh, D. M., Klyubin, I., Fadeeva, J. V., Cullen, W. K., Anwyl, R., Wolfe, M. S., Rowan, M. J., and Selkoe, D. J. (2002) Naturally secreted oligomers of amyloid β protein potently inhibit hippocampal long-term potentiation in vivo. *Nature 416*, 535−539.

(11) Haass, C., and Selkoe, D. J. (2007) Soluble protein oligomers in neurodegeneration: Lessons from the Alzheimer's amyloid β-peptide. *Nat. Rev. Mol. Cell Biol. 8*, 101−112.

(12) Serra-Vidal, B., Pujadas, L., Rossi, D., Soriano, E., Madurga, S., and Carulla, N. (2014) Hydrogen/deuterium exchange-protected oligomers populated during Aβ fibril formation correlate with neuronal cell death. *ACS Chem. Biol. 9*, 2678−2685.

(13) Fawzi, N. L., Ying, J. F., Torchia, D. A., and Clore, G. M. (2010) Kinetics of amyloid β monomer-to-oligomer exchange by NMR relaxation. *J. Am. Chem. Soc. 132*, 9948−9951.

(14) Fawzi, N. L., Ying, J., Ghirlando, R., Torchia, D. A., and Clore, G. M. (2011) Atomic-resolution dynamics on the surface of amyloid-β protofibrils probed by solution NMR. *Nature 480*, 268−272.

(15) Garvey, M., and Morgado, I. (2013) Peptide concentration alters intermediate species in amyloid β fibrillation kinetics. *Biochem. Biophys. Res. Commun. 433*, 276−280.

(16) Harper, J. D., Wong, S. S., Lieber, C. M., and Lansbury, P. T. (1999) Assembly of Aβ amyloid protofibrils: An in vitro model for a possible early event in Alzheimer's disease. *Biochemistry 38*, 8972−8980.

(17) Moreth, J., Kroker, K. S., Schwanzar, D., Schnack, C., von Arnim, C. A. F., Hengerer, B., Rosenbrock, H., and Kussmaul, L. (2013) Globular and protofibrillar Aβ aggregates impair neurotransmission by different mechanisms. *Biochemistry 52*, 1466−1476.

(18) Tay, W. M., Huang, D., Rosenberry, T. L., and Paravastu, A. K. (2013) The Alzheimer's Amyloid-β-(1−42) peptide forms off-pathway oligomers and fibrils that are distinguished structurally by intermolecular organization. *J. Mol. Biol. 425*, 2494−2508.

(19) Powers, E. T., and Powers, D. L. (2008) Mechanisms of protein fibril formation: Nucleated polymerization with competing off-pathway aggregation. *Biophys. J. 94*, 379−391.

(20) Ahmed, M., Davis, J., Aucoin, D., Sato, T., Ahuja, S., Aimoto, S., Elliott, J. I., Van Nostrand, W. E., and Smith, S. O. (2010) Structural conversion of neurotoxic amyloid-β_{1-42} oligomers to fibrils. *Nat. Struct. Mol. Biol. 17*, 561−567.

(21) Hou, L. M., Shao, H. Y., Zhang, Y. B., Li, H., Menon, N. K., Neuhaus, E. B., Brewer, J. M., Byeon, I. J. L., Ray, D. G., Vitek, M. P., Iwashita, T., Makula, R. A., Przybyla, A. B., and Zagorski, M. G. (2004) Solution NMR studies of the Aβ(1−40) and Aβ(1−42) peptides establish that the Met35 oxidation state affects the mechanism of amyloid formation. *J. Am. Chem. Soc. 126*, 1992−2005.

(22) Yan, Y. L., and Wang, C. Y. (2006) Aβ42 is more rigid than Aβ40 at the C terminus: Implications for Aβ aggregation and toxicity. *J. Mol. Biol. 364*, 853−862.

(23) Takegoshi, K., Nakamura, S., and Terao, T. (2001) ^{13}C-^{1}H dipolar-assisted rotational resonance in magic-angle spinning NMR. *Chem. Phys. Lett. 344*, 631−637.

(24) Fu, Z., Aucoin, D., Ahmed, M., Ziliox, M., Van Nostrand, W. E., and Smith, S. O. (2014) Capping of Aβ42 oligomers by small molecule inhibitors. *Biochemistry 53*, 7893−7903.

DOI: 10.1021/acs.biochem.5b00467
Biochemistry 2015, 54, 4197−4207

(25) Yamaguchi, T., Matsuzaki, K., and Hoshino, M. (2011) Transient formation of intermediate conformational states of amyloid-β peptide revealed by heteronuclear magnetic resonance spectroscopy. *FEBS Lett. 585*, 1097−1102.
(26) Kim, W., and Hecht, M. H. (2006) Generic hydrophobic residues are sufficient to promote aggregation of the Alzheimer's Aβ42 peptide. *Proc. Natl. Acad. Sci. U.S.A. 103*, 15824−15829.
(27) Cleary, J. P., Walsh, D. M., Hofmeister, J. J., Shankar, G. M., Kuskowski, M. A., Selkoe, D. J., and Ashe, K. H. (2005) Natural oligomers of the amyloid-protein specifically disrupt cognitive function. *Nat. Neurosci. 8*, 79−84.
(28) Bernstein, S. L., Dupuis, N. F., Lazo, N. D., Wyttenbach, T., Condron, M. M., Bitan, G., Teplow, D. B., Shea, J., Ruotolo, B. T., Robinson, C. V., and Bowers, M. T. (2009) Amyloid-β protein oligomerization and the importance of tetramers and dodecamers in the aetiology of Alzheimer's disease. *Nat. Chem. 1*, 326−331.
(29) Bitan, G., Kirkitadze, M. D., Lomakin, A., Vollers, S. S., Benedek, G. B., and Teplow, D. B. (2003) Amyloid β-protein (Aβ) assembly: Aβ40 and Aβ42 oligomerize through distinct pathways. *Proc. Natl. Acad. Sci. U.S.A. 100*, 330−335.
(30) Garai, K., and Frieden, C. (2005) Quantitative analysis of the time course of Aβ oligomerization and subsequent growth steps using tetramethylrhodamine-labeled Aβ. *Proc. Natl. Acad. Sci. U.S.A. 110*, 3321−3326.
(31) Mastrangelo, I. A., Ahmed, M., Sato, T., Liu, W., Wang, C., Hough, P., and Smith, S. O. (2006) High-resolution atomic force microscopy of soluble Aβ42 oligomers. *J. Mol. Biol. 358*, 106−119.
(32) Vivekanandan, S., Brender, J. R., Lee, S. Y., and Ramamoorthy, A. (2011) A partially folded structure of amyloid-β (1−40) in an aqueous environment. *Biochem. Biophys. Res. Commun. 411*, 312−316.
(33) Bolognesi, B., Kumita, J. R., Barros, T. P., Esbjorner, E. K., Luheshi, L. M., Crowther, D. C., Wilson, M. R., Dobson, C. M., Favrin, G., and Yerbury, J. J. (2010) ANS binding reveals common features of cytotoxic amyloid species. *ACS Chem. Biol. 5*, 735−740.
(34) Cerf, E., Sarroukh, R., Tamamizu-Kato, S., Breydo, L., Derclaye, S., Dufrene, Y. F., Narayanaswami, V., Goormaghtigh, E., Ruysschaert, J. M., and Raussens, V. (2009) Antiparallel β-sheet: A signature structure of the oligomeric amyloid β-peptide. *Biochem. J. 421*, 415−423.
(35) Sarroukh, R., Cerf, E., Derclaye, S., Dufrene, Y. F., Goormaghtigh, E., Ruysschaert, J. M., and Raussens, V. (2011) Transformation of amyloid β(1−40) oligomers into fibrils is characterized by a major change in secondary structure. *Cell. Mol. Life Sci. 68*, 1429−1438.
(36) Barth, A. (2007) Infrared spectroscopy of proteins. *Biochim. Biophys. Acta 1767*, 1073−1101.
(37) Paul, C., Wang, J. P., Wimley, W. C., Hochstrasser, R. M., and Axelsen, P. H. (2004) Vibrational coupling, isotopic editing, and β-sheet structure in a membrane-bound polypeptide. *J. Am. Chem. Soc. 126*, 5843−5850.
(38) Petty, S. A., and Decatur, S. M. (2005) Experimental evidence for the reorganization of β-strands within aggregates of the Aβ(16−22) peptide. *J. Am. Chem. Soc. 127*, 13488−13489.
(39) Masuda, Y., Uemura, S., Nakanishi, A., Ohashi, R., Takegoshi, K., Shimizu, T., Shirasawa, T., and Irie, K. (2008) Verification of the C-terminal intramolecular β-sheet in Aβ42 aggregates using solid-state NMR: Implications for potent neurotoxicity through the formation of radicals. *Bioorg. Med. Chem. Lett. 18*, 3206−3210.
(40) Sato, T., Kienlen-Campard, P., Ahmed, M., Liu, W., Li, H., Elliott, J. I., Aimoto, S., Constantinescu, S. N., Octave, J. N., and Smith, S. O. (2006) Inhibitors of amyloid toxicity based on β-sheet packing of Aβ40 and Aβ42. *Biochemistry 45*, 5503−5516.
(41) Jeong, J. S., Ansaloni, A., Mezzenga, R., Lashuel, H. A., and Dietler, G. (2013) Novel mechanistic insight into the molecular basis of amyloid polymorphism and secondary nucleation during amyloid formation. *J. Mol. Biol. 425*, 1765−1781.
(42) Gu, L., Liu, C., Stroud, J. C., Ngo, S., Jiang, L., and Guo, Z. (2014) Antiparallel triple-strand architecture for prefibrillar Aβ42 oligomers. *J. Biol. Chem. 289*, 27300−27313.
(43) Torok, M., Milton, S., Kayed, R., Wu, P., McIntire, T., Glabe, C. G., and Langen, R. (2002) Structural and dynamic features of Alzheimer's Aβ peptide in amyloid fibrils studied by site-directed spin labeling. *J. Biol. Chem. 277*, 40810−40815.
(44) Sciarretta, K. L., Gordon, D. J., Petkova, A. T., Tycko, R., and Meredith, S. C. (2005) Aβ 40-Lactam(D23/K28) models a conformation highly favorable for nucleation of amyloid. *Biochemistry 44*, 6003−6014.
(45) Sandberg, A., Luheshi, L. M., Sollvander, S., de Barros, T. P., Macao, B., Knowles, T. P. J., Biverstal, H., Lendel, C., Ekholm-Petterson, F., Dubnovitsky, A., Lannfelt, L., Dobson, C. M., and Hard, T. (2010) Stabilization of neurotoxic Alzheimer amyloid-β oligomers by protein engineering. *Proc. Natl. Acad. Sci. U.S.A. 107*, 15595−15600.
(46) Hard, T. (2011) Protein engineering to stabilize soluble amyloid β-protein aggregates for structural and functional studies. *FEBS J. 278*, 3884−3892.
(47) O'Nuallain, B., Freir, D. B., Nicoll, A. J., Risse, E., Ferguson, N., Herron, C. E., Collinge, J., and Walsh, D. M. (2010) Amyloid β-protein dimers rapidly form stable synaptotoxic protofibrils. *J. Neurosci. 30*, 14411−14419.

DOI: 10.1021/acs.biochem.5b00467
Biochemistry 2015, 54, 4197−4207